Figure 11 Photograph of the (a) daughter board and (b) backplane. [Color figure can be viewed in the online issue, which is available at www.interscience.wiley.com.]

4.5. LVDS signals, ground/power, and TTL signals in the daughter boards and backplane are placed in different layers, respectively, so that the TTL and LVDS signals will be isolated by the ground/power plane(s) in order to minimize the noise coupling into LVDS signals from the large-swing TTL signals. A photograph of the daughter board and backplane in the demo system is shown in Figure 11.

All the active devices are placed on daughter boards that transmit and receive the LVDS and TTL data streams. The circuit on the daughter boards is uniformity designed, but different functions (Tx or Rx) are approached by means of programming and provided with compatibility [9, 10]. A passive backplane is designed with various interconnects according to the requirement for investigating the SI issue of different interconnects.

Point-to-point LVDS links are used for data transmission in the demo system for obtaining the perfect transfer performance and SI investigation. The unidirectional transmission of 10 pairs of the LVDS links group is used for the LVDS group data transmission in the demo system, which involves eight data pairs, a clock pair, and a frame pair [11]. The DDR operation mode is used for the LVDS clock. Each pair of LVDS links with the transmission rate of 500 M/bs is designed for a 250-MHz clock frequency. The throughput of 4 Gb/s is provided to each group of LVDS.

CONCLUSION

In this paper, the SI analysis of high-speed digital systems has been systematically performed using the full-wave electromagnetic analysis method. From the simulated and measured results, we can observe that high-speed digital signals at 500 M/bs can be smoothly transmitted in the designed long interconnects on the backplane. Transmission-line discontinuities generate the main problems, which cause signal degradation for high-speed signal transfer on PCBs. Such discontinuities can be sharp bends on the trace, skews between conductors within a differential pair, and vias through the board. In the other words, these discontinuities are points that cause impedance discontinuities of the transmission line, which cause reflections. The following layout rules for transmission lines are summarized to enhance board operation: avoid 90° turns and use arcs or 45° bevels. The distance between two traces should remain constant in order to avoid discontinuities in differential impedance. If vias cannot be avoided, use as few as possible.

ACKNOWLEDGMENT

REFERENCES

1. R.Y. Chen, Engineering electromagnetic compatibility, 2nd ed., IEEE Press and Wiley, Hoboken, NJ, 2001, ch. 14.
2. H.W. Johnson and M. Graham, High-speed digital design, Prentice Hall, Englewood Cliffs, NJ, 2001.
3. LVDS owner's manual design guide, National Semiconductor, 1997.
4. R.H.G. Cuny, SPICE and IBIS modeling kits: The basis for signal integrity analyses, IEEE Intl Symp Electromagn Compat 8 (1996), 204–208.
5. L. Walling and S. Polstyanko, Solving a high-frequency signal-integrity problem, Microwaves RF 39 (2000), 63–66.
6. K. Kurokawa, Power waves and the scattering matrix, IEEE Trans Microwave Theory Tech 13 (1965), 194–202.
7. D.E. Bockelman and W.R. Eisenstadt, Combined differential and common-mode scattering parameters: Theory and simulation, IEEE Trans Microwave Theory Tech 43 (1995), 1530–1539.
8. D.E. Bockelman and W.R. Eisenstadt, Pure-mode network analyzer for on-ware measurements of mixed-mode S-parameters of differential circuits, IEEE Trans Microwave Theory Tech 45 (1997), 1071–1077.
9. W. Wang, Design and implementation of the high-speed digital circuit demo system, M.Sc. dissertation, Southeast University, 2004.
10. J. Hu, LVDS signal integrity (SI) analysis and high-speed backplane design, M.Sc. dissertation, Southeast University, 2004.
11. E. McGettigan, Eight channel, one clock, one frame LVDS transmitter/receiver, XILINX, 2001.

CONVERGENCE OF GAUSSIAN-BEAM MODES IN CORRUGATED CONICAL HORNS

F. Martín-Jiménez,[1] E. García,[2] C. O'Sullivan,[3] L. De Haro,[4] J. A. López Fernández,[5] F. Tercero,[5] M. Sierra-Castañer,[4] and J. Martín-Pintado[1]
[1] Departamento de Estructura de la Materia
C.S.I.C., Spain
[2] Departamento de Teoría de la Señal y Comunicaciones
Universidad Carlos III de Madrid
Avda. de la Universidad 30
28911, Leganés, Madrid, Spain
[3] Dept. of Experimental Physics
National University of Ireland, Maynooth
Maynooth, Co. Kildare, Ireland
[4] Centro Astronómico de Yebes
Instituto Geográfico Nacional
Yebes, Guadalajara, Spain
[5] Centro Astronomico de Yebes Observatorio Astronomico Nacional
Yebes, Spain

ABSTRACT: *Gaussian beam-mode expansion with only the fundamental mode does not work properly when the angular region of interest is wide. It is necessary to use higher-order mode for the expansion. A study of the convergence of these higher order modes is presented for the case of a corrugated conical horn. Conclusions about the number of modes necessary for good accuracy are given. © 2005 Wiley Periodicals, Inc. Microwave Opt Technol Lett 45: 199–203, 2005; Published online in Wiley InterScience (www.interscience.wiley.com). DOI 10.1002/mop. 20769*
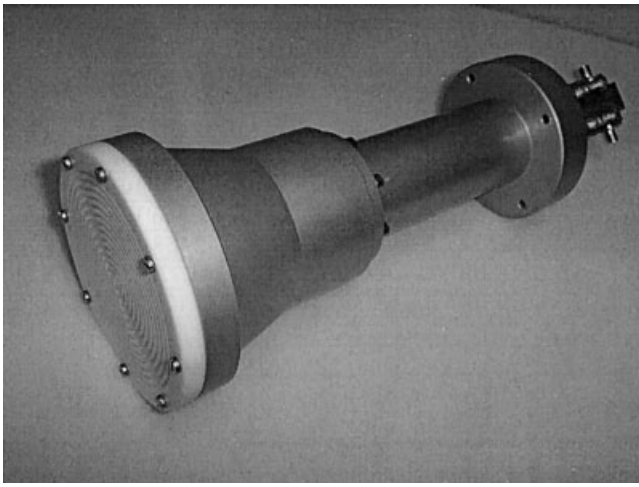
Figure 1 Corrugated conical horn with lens

TABLE 1 Coefficients for the Beam-Mode Expansion of a Corrugated Conical Horn with W/a = 0.6435

A_0	1.13	A_{21}	$-4.74 \cdot 10^{-3}$
A_1	$-3.38 \cdot 10^{-5}$	A_{22}	$-2.704 \cdot 10^{-3}$
A_2	-0.137	A_{23}	$-3.879 \cdot 10^{-4}$
A_3	-0.049	A_{24}	$-1.715 \cdot 10^{-3}$
A_4	0.022	A_{25}	$3.246 \cdot 10^{-3}$
A_5	0.039	A_{26}	$4.019 \cdot 10^{-3}$
A_6	0.023	A_{27}	$4.012 \cdot 10^{-3}$
A_7	$2.185 \cdot 10^{-4}$	A_{28}	$3.333 \cdot 10^{-3}$
A_8	-0.014	A_{29}	$2.187 \cdot 10^{-3}$
A_9	-0.017	A_{30}	$8.143 \cdot 10^{-4}$
A_{10}	-0.012	A_{31}	$-5.494 \cdot 10^{-4}$
A_{11}	$-3.322 \cdot 10^{-3}$	A_{32}	$-1.705 \cdot 10^{-3}$
A_{12}	$4.424 \cdot 10^{-3}$	A_{33}	$-2.512 \cdot 10^{-3}$
A_{13}	$8.881 \cdot 10^{-3}$	A_{34}	$-2.901 \cdot 10^{-3}$
A_{14}	$9.541 \cdot 10^{-3}$	A_{35}	$-2.866 \cdot 10^{-3}$
A_{15}	$7.196 \cdot 10^{-3}$	A_{36}	$-2.458 \cdot 10^{-3}$
A_{16}	$3.246 \cdot 10^{-3}$	A_{37}	$-1.77 \cdot 10^{-3}$
A_{17}	$-8.815 \cdot 10^{-4}$	A_{38}	$-9.171 \cdot 10^{-4}$
A_{18}	$-4.099 \cdot 10^{-3}$	A_{39}	$-1.815 \cdot 10^{-5}$
A_{19}	$-5.820 \cdot 10^{-3}$	A_{40}	$8.155 \cdot 10^{-4}$
A_{20}	$-5.95 \cdot 10^{-3}$		

1. INTRODUCTION

Throughout history, human beings have been interested in knowing about what exists far away in the sky. Beginning with the ancient Greeks, and continuing with the telescope of Galileo up to the various advances in the 20th century, many instruments for astronomical research have been developed in order to satisfy this interest.

The last of these instruments, and probably the most powerful, is the radio telescope. Quasi-optical theory has been commonly used in the design of the various parts of these devices due to the potential for using Gaussian-beam mode expansion (BME) to focalise the instruments.

Generally, the use of the Gaussian BME is reduced to the use of the fundamental mode of the expansion, but higher modes are not included in the development. Designs based on the fundamental mode are simpler and work properly when the beam pattern is studied in a narrow angular range. Unfortunately, when this range increases, the design fails. In fact, the fundamental mode cannot properly expand the secondary lobes of the radiating elements as the radio-telescope feed can. Accordingly, in cases where the required angular range is increased, it is important to know the number of modes to use. Knowing the convergence of these modes helps to determine this number.
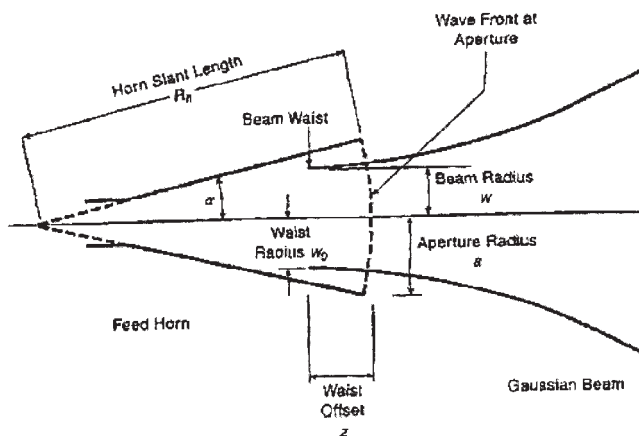
2. QUASI-OPTICAL THEORY

One of the most widely agreed-upon definition of quasi-optics is that it deals with the propagation of reasonably well-collimated beams, although they have small dimensions in the direction transversal to the axis of propagation, which is measured in wavelengths. Thus, this theory is suitable to the important and common case of beams with diameters that are not too large in wavelengths, such as Gaussians beams [1]. These beams can be used to expand the radiation emitted by different types of sources in a sum of Gaussian modes (BME), that notably simplifies the design of RF elements and systems in the millimetre and submillimetre band, such as radiotelescope systems.

The main advantages of this theory, which was developed by Goldsmith [1], are as follows:

- it allows us to skip using dielectric or metallic lines as the transmission medium, hence, keeping the dimensions of the components within feasible limits and decreasing losses;
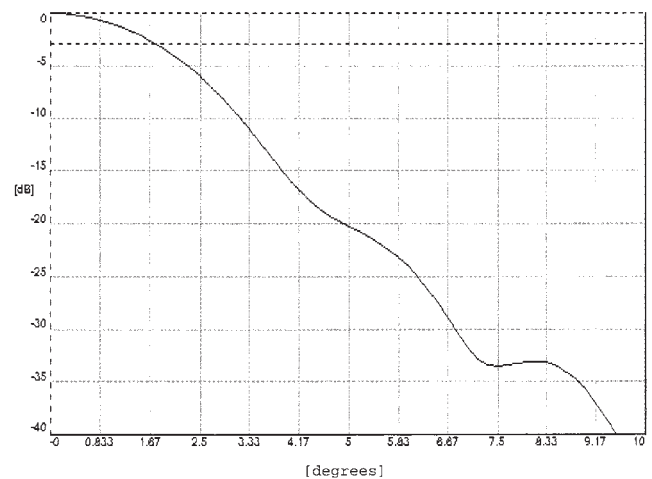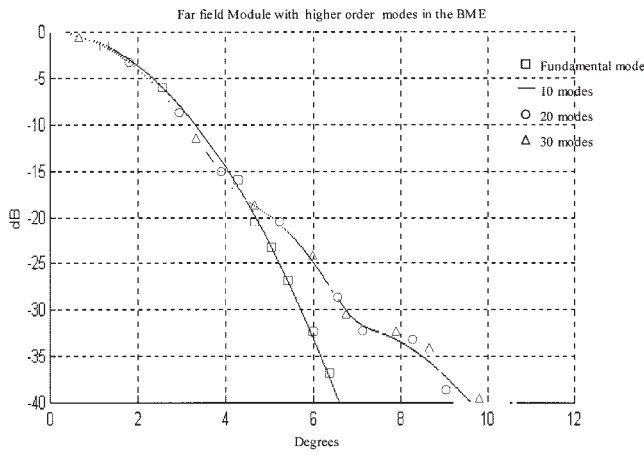

Figure 2 Scheme of a corrugated conical horn

Figure 3 Field for the corrugated conical horn simulated, obtained with SABOR

Figure 4 Field produced by the corrugated conical horn expanded into Gaussian-beam modes (squares: only fundamental mode, continuous line: 10 modes, triangles: 20 modes, circles: 30 modes)

- it can be applied to several polarizations and wide bandwidths;
- it makes expanding the power transmitted in a region of several wavelengths possible, whereas the monomode transmission lines are restrained to the wavelength as maximum;
- quasi-optical systems are flexible, since the same set of components (lens, mirrors, and so on) can operate with different beams in an individual way. This allows a better use of the available space in the radio-telescope cabinet, which is limited.

2. BEAM MODE EXPANSION OF CORRUGATED CONICAL HORNS

Corrugated conical horns, like the one shown in Figure 1, are commonly used as the feed for quasi-optical systems such as radio-telescope ones [2, 3]. These horns, when properly built, produce at their aperture a hybrid mode HE_{11} and a rotationally symmetric field expressed as follows:

$$E_x(r) = 0, \qquad E_y(r) = A J_0^T(k_c r) \exp\left(\frac{-jk_0 r^2}{2R_h}\right), \qquad (1)$$
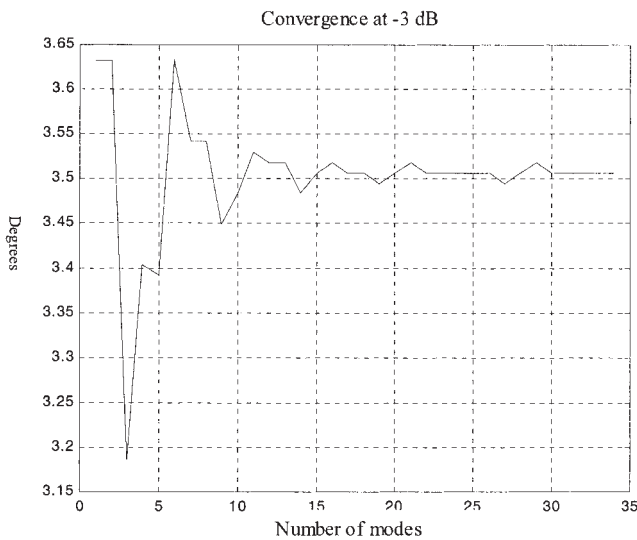
Figure 5 Convergence of Gaussian-beam modes for a corrugated conical horn at −3 dB
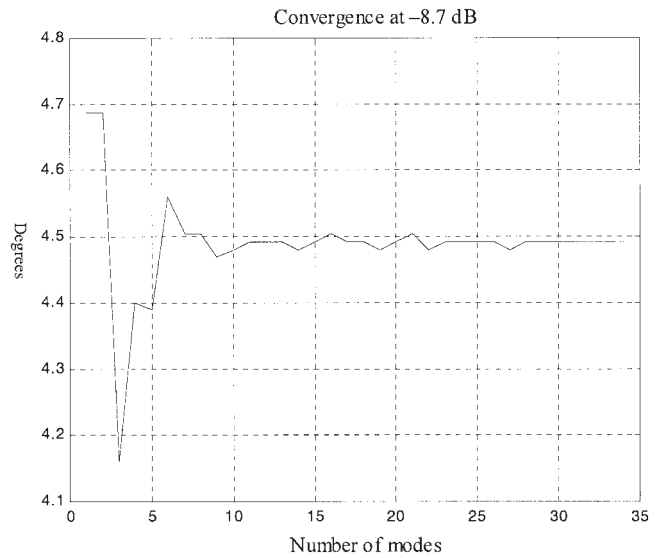
Figure 6 Convergence of Gaussian-beam modes for a corrugated conical horn at −8.7 dB
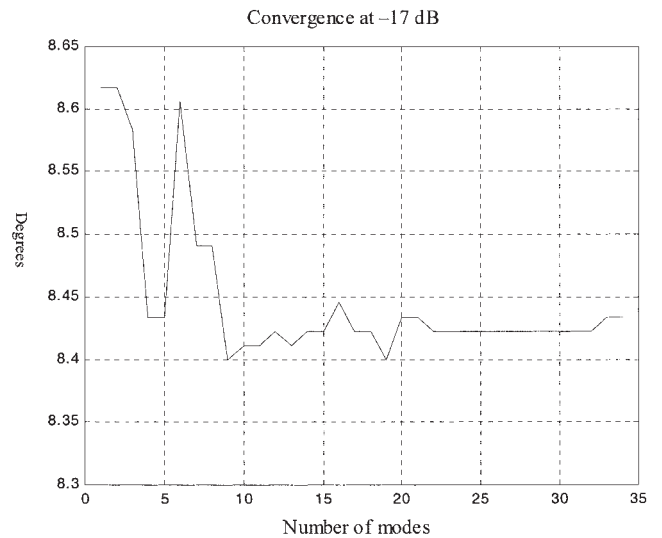
where

$$r^2 = x^2 + y^2 \qquad k_c = \frac{2.405}{a}$$

where a = aperture radius,

$$k_0 = 2 \cdot \pi/\lambda_0, \qquad J_0^T(x) = \begin{cases} J_0(x) \rightarrow x < 2.405 \\ 0 \rightarrow x > 2.405 \end{cases},$$

and R_h is the curvature radius of the equal-phase plane that includes the aperture of the horn and considers the horn vertex as the phase centre (see Fig. 2).

In [4], Wylde presented the BME for the field radiated by these kind of horns using only Gaussian rotationally symmetric modes (modes $m = 0$):

Figure 7 Convergence of Gaussian-beam modes for a corrugated conical horn at −17 dB

$$E(r, z) = \sum_{p=0}^{\infty} A_p \left(\frac{2}{\pi w^2} \right)^{0.5} L_{0p} \left[\frac{2r^2}{w^2} \right]$$

$$\times \exp\left(-j\left(\frac{k_0 r^2}{2q(z)} \right) + \phi_p(z) \right) \exp(jk_0 z), \quad (2)$$

where A_p denotes the amplitude coefficients that can be obtained by fixing a condition of power distribution of the modes that is related with the beam radius at the aperture over the aperture radius (W/a). Seeking to couple the most power in the fundamental mode ($p = 0$), Wylde obtained a relation $W/a = 0.6435$ with a fraction of power transmitted in the fundamental mode of $\eta = 0.9792$. For these conditions, the coefficients obtained are listed in Table 1.

The fundamental mode obtains a good approximation for the main lobe of the field, but when the angular range under study increases it is necessary to use higher-order modes. Obviously, the use of higher-order modes makes the calculus more complex. As a result, it is important to achieve a compromise between accuracy and calculus complexity. For this purpose, a study has been developed about Gaussian-mode convergence in corrugated conical horns, specifically, looking for the ideal number of modes.

The field produced by a simulated corrugated conical horn has been studied with the following features: frequency = 22 GHz, F/D = 7.9, taper = −12 dB, β = 1.5079, aperture radius = 147.683 mm, axial length = 3328.99 mm, slant length = 3332.27 mm, z_c = 1497.03 mm, offset waist-aperture = 943.763 mm, and beam waist = 80.6101 mm.

The method used for this study consisted in applying BME to the field radiated by this horn, thus truncating the summa with different number of modes from the fundamental mode to 34 modes. For each one of these expanded fields, the beam width has been obtained at different power levels, depending on the convergence of the obtained values.

3. RESULTS

Figure 3 shows the field produced by this horn obtained using the SABOR software for antenna design, which proved satisfactory in multiple designs [5]. Figure 4 depicts the same field obtained using a different number of modes. How the number of modes affects the
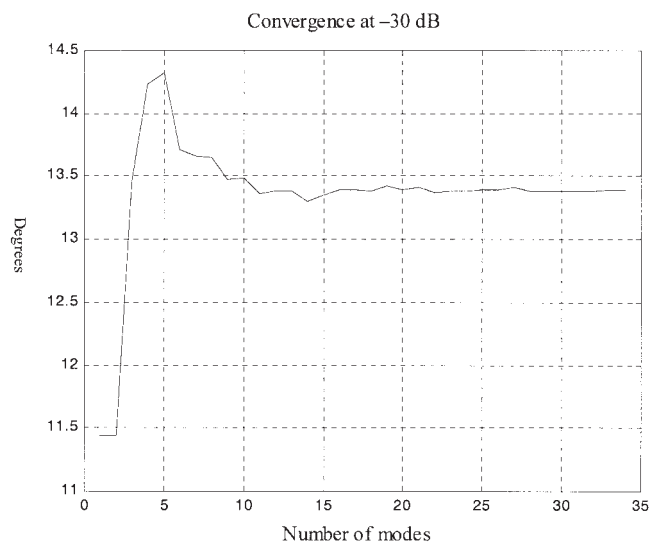
Figure 8 Convergence of Gaussian-beam modes for a corrugated conical horn at −30 dB
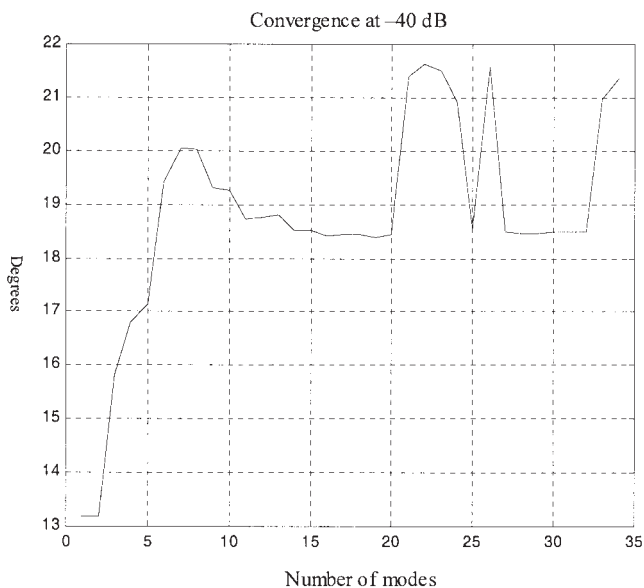
Figure 9 Convergence of Gaussian-beam modes for a corrugated conical horn at −40 dB

fields obtained can be observed, especially at the secondary lobes and for low power levels. It is concluded that for levels higher than −30 dB, the expansions are similar for more than 10 modes. However, for lower levels, the differences are higher; thus, it is complicated to approximate the lobe at 8°. Moreover, for these levels the paraxial approximations begin to fail.

Figure 5 presents the variation of the beam width at −3 dB. It can be observed that for expansions with less than nine modes the variations are very significant. For expansions with more than 10 modes, the variations are lower; meanwhile, for more than 25, convergence is assured.

Figure 6 shows the same variation, but now at −8.7 dB, which is equivalent to the beam radius. In this case, the variations are important for less than 10 modes.

Figure 7 depicts the beam width at −17 dB, which coincides with the second lobe. Again, the variations are important for expansions with less than 10 modes, but now it can be observe that from 15 to 20 modes there is a variation of 0.5°. For more than 20 modes, it can be considered that the expansion has converged.

Figure 8 presents the differences for −30 dB. At this level the paraxial approximation may fail, but the results show that the convergence is reached for 15 modes.

Figure 9 shows the variation for −40 dB. It can be observed that the convergence is not clear and there are oscillations. This result is a consequence of what is depicted in Figure 3: the problems for the lobe at 8°. Depending of the number of modes, this lobe is approximated in a different manner. In any case, it must be said that at this level is difficult to measure properly.

4. CONCLUSION

It can be concluded from Figures 5–8 that the convergence of Gaussian modes is quite fast. In almost every case, convergence has been reached with 10 modes. Only in one case, at −17 dB, convergence is reached at −20 dB; thus, for a conservative design, 20 modes ensures convergence.

Also, Figure 3 demonstrates that for levels higher than −30 dB, convergence is reached quickly. However, for levels lower than −30 dB, convergence is not assured, since the paraxial approximation starts failing.

REFERENCES

1. P.F. Goldsmith, Quasioptical systems, IEEE Press and Chapman & Hall Publishers Series on Microwave Technology and Rf. 1997.
2. J.A. Murphy, Apperture efficiencies of large axisymetric reflector antennas fed by conical horns, IEEE Proc Antennas Propagat 36 (1988).
3. M. Carter and J.W. Lamb, Proposal for a new layout for the receiver cabin of the 30-m telescope at Pico Veleta, IRAM, Grenoble, 1995.
4. R.J. Wylde, M.A., and A.M.I.E.E., Millimetre-wave Gaussian beam-mode optics and corrugated feed horns, IEEE Proc Antennas Propagat 131 (1984).
5. M.A. Campo, F.J. Del Rey, J.L. Besada, and L. de Haro, SABOR: Description of the methods applied of horn and reflector antennas, IEEE Antennas Propagat Mag 40 (1998), 95–108.
6. E. García, J.A. López Fernández, L. de Haro, F. Tercero, B. Galocha, A. Barcia, and J.L. Besada, Analysis of the defocused Gaussian beam telescope on cassegrain feeds, Microwave Opt Technol Lett 32 (2002), 420–423.

A NEW LOOK AT FDTD EXCITATION SOURCES

Tao Su, Wenhua Yu, and Raj Mittra
Electromagnetic Communication Laboratory, 319 EE East
The Pennsylvania State University
University Park, PA 16802

ABSTRACT: *In FDTD simulations, the excitation sources can be divided into two categories: (i) the displacement-current source, which is generated by a time-varying electric field; (ii) the induced-current source, which exists in the lossy material. Currently, the latter source is the popular choice in most FDTD simulations. However, there are two problems with the use of this source: the time signal shape at the observation points is different from that of the input pulse, and an artificial DC component is introduced into the solution that prevents the solution from converging to zero. The objective of this paper is to investigate these excitation sources and to clarify some concepts in FDTD simulations.* © 2005 Wiley Periodicals, Inc. Microwave Opt Technol Lett 45: 203–207, 2005; Published online in Wiley InterScience (www.interscience.wiley.com). DOI 10.1002/mop. 20770

1. INTRODUCTION

The finite-difference time-domain (FDTD) method employing the Yee algorithm [1] has enjoyed a long history of success in computational electromagnetics. Much progress has been made in improving the original Yee algorithm by introducing absorbing boundary conditions [2–4], conformal techniques [5–7], subgridding approaches [8–10], and so forth, and in applying the FDTD to a variety of applications [11–13]. The excitation source, similar to the absorbing boundary for mesh truncation and the conformal technique for handling arbitrary objects, plays a very important role in FDTD simulations; however, the choice of the source has not received as much attention as the others. The induced-current source, which only exists in a lossy medium, is frequently used in FDTD simulations even though the source is located in free space. Such a source generates artificial electrical charges, which produce the so-called DC component in the solution [13]. The actual charge accumulation in a lossy medium survives only during the relaxation time. However, the artificial charges caused by this current source in free space lasts indefinitely. The implementation and physical explanation of the induced current source have been discussed in [14]. In order to eliminate the DC component from the solution, there are at least two excitation sources [15, 16] that have been introduced into FDTD simulation. These excitation sources without the DC component have complicated expressions, compared to the Gaussian pulse. These sources cannot be used as a reference for normalization because both the electrical and magnetic fields at the observation points are different from the input current pulse in both the time and frequency domains. Unlike the induced current source, the displacement current in Maxwell's equations can exist in free space. Although in most cases we can obtain the same results from these two different excitation sources, the displacement current source has the following advantages over the induced current source: (i) it does not generate a DC component in the FDTD solution, therefore, the solution always converges to zero; (ii) the pulse shape measured at an observation point is identical to that of the input pulse. Because the displacement-current source is realized through a time-varying electric field, the received electric field at an observation point has the same pulse shape as the excitation electric field. For such sources, the fields inside the source location appear in Maxwell's updating. In contrast, the fields inside the source are not updated in the so-called "hard source," until after the excitation has gone to zero. Although the hard source does not suffer from the DC bias problem of the displacement current source, it does have two shortcomings: (i) the source has to be terminated at the end of its life span; (ii) it fails to handle the scattered field arriving at the source region before the end of the source excitation. In this paper, we first investigate the induced current source and then introduce the concept of the displacement current sources in the FDTD simulations.

2. INDUCED CURRENT SOURCE

We begin with the Maxwell's equation and continuity conditions, expressed as

$$\nabla \times \vec{H} = \varepsilon_0 \frac{\partial \vec{E}}{\partial t} + \vec{J}, \qquad (1)$$

$$\nabla \cdot \vec{J} = -\frac{\partial \rho}{\partial t}. \qquad (2)$$
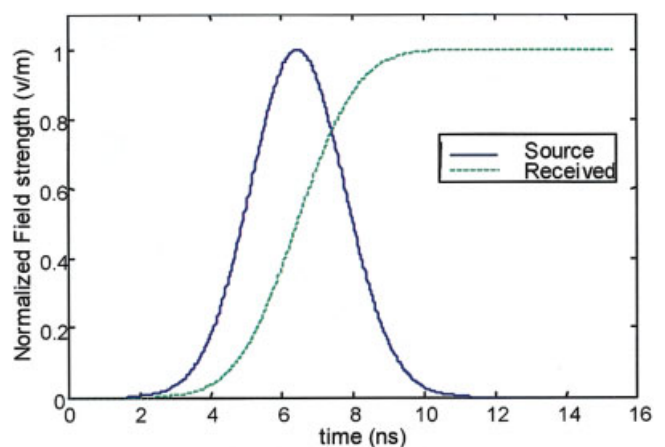
Figure 1 Charge deposited at the ends of dipole vs. time. [Color figure can be viewed in the online issue, which is available at www. interscience.wiley.com.]